

**Analyzing Type IIn Supernovae spectra to determine if  
some arise from runaway luminous blue variable stars**

**A THESIS  
SUBMITTED TO THE FACULTY OF THE GRADUATE SCHOOL  
OF THE UNIVERSITY OF MINNESOTA  
BY**

**Michael Makmur**

**IN PARTIAL FULFILLMENT OF THE REQUIREMENTS  
FOR THE DEGREE OF  
MASTER OF SCIENCE**

**Patrick L. Kelly**

**May, 2020**

© Michael Makmur 2020  
ALL RIGHTS RESERVED

# Acknowledgements

tbd

The data presented herein were obtained at the W. M. Keck Observatory, which is operated as a scientific partnership among the California Institute of Technology, the University of California and the National Aeronautics and Space Administration. The Observatory was made possible by the generous financial support of the W. M. Keck Foundation.

The author wishes to recognize and acknowledge the very significant cultural role and reverence that the summit of Maunakea has always had within the indigenous Hawaiian community. We are most fortunate to have the opportunity to use observations from this mountain.

This research has made use of the Keck Observatory Archive (KOA), which is operated by the W. M. Keck Observatory and the NASA Exoplanet Science Institute (NExScI), under contract with the National Aeronautics and Space Administration.

# Dedication

tbd

## **Abstract**

# Contents

<b>Acknowledgements</b>	<b>i</b>
<b>Dedication</b>	<b>ii</b>
<b>Abstract</b>	<b>iii</b>
<b>List of Tables</b>	<b>vi</b>
<b>List of Figures</b>	<b>vii</b>
<b>1 Introduction</b>	<b>1</b>
1.1 Supernovae . . . . .	1
1.1.1 Types of SNe . . . . .	1
1.1.2 Type IIn Supernovae . . . . .	2
1.2 Runaway Stars . . . . .	6
1.3 This thesis . . . . .	9
<b>2 Observations</b>	<b>10</b>
2.1 Observed SNe IIn . . . . .	10
2.2 DEIMOS . . . . .	10
2.3 H $\alpha$ $\lambda$ 6562 . . . . .	12
<b>3 Analysis</b>	<b>14</b>
3.1 Reducing DEIMOS Images . . . . .	14
3.2 Analyzing Velocities of SNe IIn . . . . .	15

<b>4 Discussion</b>	<b>17</b>
4.1 Runaway Candidates . . . . .	17
4.1.1 SN 2010jl . . . . .	17
4.1.2 SN 2013dz . . . . .	18
4.2 Implications on progenitors . . . . .	19
<b>5 Conclusion</b>	<b>21</b>
<b>Appendix A. Glossary and Acronyms</b>	<b>27</b>
A.1 Glossary . . . . .	27
A.2 Acronyms . . . . .	28
<b>Appendix B. Images and Spectra</b>	<b>29</b>

# List of Tables

2.1	Table of observations . . . . .	11
3.1	List of SNe IIn, the FWHM of their H $\alpha$ emission, and their offset velocities from their host galaxies. . . . .	16
A.1	Acronyms . . . . .	28

# List of Figures

1.1	Cartoon of the basic structure for a SN IIn	3
1.2	Plot comparing mass-loss rate and wind velocities of SN IIn to possible progenitors	5
1.3	Plot depicting how far a runaway star will travel before exploding in a SN	8
2.1	Image of SN 2015bf from DEIMOS	11
2.2	Spectrum of the H $\alpha$ emission from SN 2008en	12
2.3	H $\alpha$ emission from SN 2013dz and its host galaxy	13
4.1	Spectrum of the H $\alpha$ emission from SN 2010jl	18
4.2	1-D spectrum of SN 2013dz taken by DEIMOS	20
B.1	SN 2005R H $\alpha$ relative to host galaxy	29
B.2	SN 2008en H $\alpha$ relative to host galaxy	30
B.3	SN 2010jl H $\alpha$ relative to host galaxy	30
B.4	SN 2012ab H $\alpha$ relative to host galaxy	31
B.5	SN 2013dz H $\alpha$ relative to host galaxy	31
B.6	SN 2013W H $\alpha$ relative to host galaxy	32

# Chapter 1

## Introduction

### 1.1 Supernovae

When stars reach the end of their lives, they will either go with a bang or a whimper depending on their initial masses. Stars that start with less than 8 solar masses ( $M_{\odot}$ ) at birth tend to fall into the latter category, releasing their outer layers into a planetary nebula and leaving their collapsed cored as a white dwarf star. Stars more massive than  $8M_{\odot}$ , on the other hand, fall in the former category. These stars will undergo a sudden core collapse, with the resulting explosion   several solar masses of outer layers at extreme speeds while the core collapses into a neutron star or, if massive enough, a black hole. These events are called supernovae (SNe, singular supernova/SN), and can be some of the most luminous transient events in astronomy<sup>1</sup>.

#### 1.1.1 Types of SNe

There are two main types of SN which are distinguished by the presence or lack of hydrogen in their spectra - Type I SNe lack hydrogen emission while Type II have it present. Each type is further divided into subtypes. Type I SNe are divided between Type Ia which has a silicon absorption feature, while Types Ib/c do not (these are split based on the presence of a He I line at 5876 Å). Type II SNe are divided in four

---

<sup>1</sup> The core collapse supernova (CCSN, plural CCSNe) describes this event, but white dwarfs can also undergo supernova. If a white dwarf accretes enough mass to pass the Chandrasekhar limit ( $1.4M_{\odot}$ ), it will undergo runaway nuclear fusion and explode as a Type Ia SN (spectrum described in Sec. 1.1.1).

main ways:

- Type I Ib SNe lose their hydrogen emission over time and become similar to SNe Ib
- Type II In SNe show narrow lines of hydrogen emission
- Type II-L SNe show a linear decrease in their light curve, and have no narrow lines
- Type II-P SNe show an extended period of luminosity (a “plateau” in their light curve, hence the “P”) before decreasing in brightness.

In this thesis we take a specific eye towards Type II In SNe, though as will be seen they may actually arise from the other subtypes of SN 

### 1.1.2 Type II In Supernovae

Type II In supernovae (SNe II In) are a subclass of CCSNe which show strong, narrow Balmer lines of hydrogen in their spectra (Schlegel, 1990),  making up approximately 10% of all CCSNe. It is expected that these narrow lines arise from the supernova shock interacting with a dense, pre-existing circumstellar medium (CSM) surrounding the progenitor star (Smith, 2017), though the exact origins of the CSM is still up for debate. No matter the progenitor, some sort of extreme mass-loss is required in the decades prior to the explosion in order to generate such a CSM.

Because of the dense, surrounding CSM, the basic structure of a SNe II In differs significantly from other SNe. As seen in Fig. 1.1, Smith (2017) splits the SN II In into four physical zones: the unshocked CSM (1), the shocked CSM (2), the shocked SN ejecta (3), and the freely expanding SN ejecta (4). At the boundaries of each zone are the forward and reverse shocks, as well as the cold dense shell (CDS) between zones 2 and 3. In a non-SNe II In, an observer would see radiation emerging almost entirely from zone 4, but since the CSM is so dense for these explosions, each zone can provide significant contributions towards emitted radiation (Smith, 2017). As the explosion progresses and the photosphere recedes into zones 2 and 3, the gas piled into the CDS is constantly reheated by the shock and emits strong H $\alpha$  intermediate-width lines.

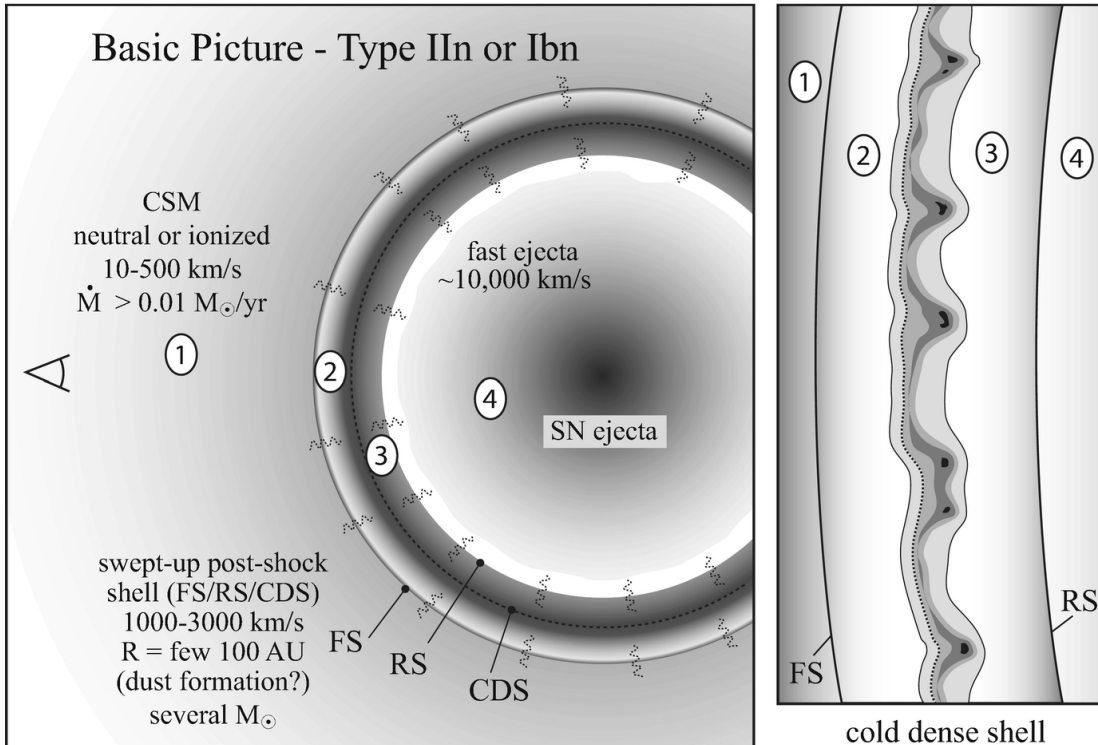


Figure 1.1: Cartoon of the basic structure of a SNe IIn. SNe IIn can be split into four separate zones: (1) the unshocked CSM, (2) the shocked CSM, (3) the shocked SN ejecta, and (4) freely expanding SN ejecta. At each boundary is a different event: between (1) and (2) exists the forward shock, between (2) and (3) is the cold dense shell (CDS), and between (3) and (4) is the reverse shock. X-rays and UV radiation can also be generated by the shock and propagate forwards into the CSM or back into the SN ejecta, and this is represented by the squiggly lines. This figure has been adapted from Smith et al. (2008).

It is important to remember that SNe IIn are an *external* phenomenon - they may actually mask other types of supernovae. Any type of core collapse supernova or even thermonuclear supernova can create the narrow Balmer lines seen in SNe IIn, so long as there is a dense enough hydrogen-rich medium surrounding the explosion (Smith, 2017). Because of this, it is impossible to trace SNe IIn to a single type of progenitor star or explosion type. SNe IIn could be covering up a SNe II-b, II-L, or II-P, and because of the dense CSM it is impossible to know what the explosion type truly is. There are also Type Ibn SNe (referenced in Fig. 1.1) which display prominent narrow helium lines, as well as Type Ia-CSM SNe which show signs of a dense CSM surrounding the thermonuclear SNe.

The luminosity of an SN IIn can be used to obtain information about the mass-loss rate of the progenitor star (Smith, 2017), allowing observers to determine other properties of the progenitor. SNe IIn can end up being much more luminous than other SNe, as the radiative shock from CSM interaction is extremely efficient at transforming the kinetic energy of the SN shockwave into visible-wavelength light (Smith, 2017). Because the luminosity is directly tied to the CSM, it can be expressed as

$$L = \frac{1}{2}wV_{\text{CDS}}^3 \quad (1.1)$$

where  $w$  represents the wind density parameter,  $w = \dot{M}/V_{\text{CSM}}$ , and  $V_{\text{CDS}}$  is the speed of the cold dense shell, the contact discontinuity where the SN shock and CSM meet (Smith, 2017).  $V_{\text{CDS}}$  can be estimated from the full width half maximum (FWHM) of intermediate-width lines in the optical spectrum, while  $V_{\text{CSM}}$ , the velocity of the CSM untouched by the SN shock, can be measured from narrower components. Combining this together, the mass-loss rate of the progenitor can be estimated by

$$\dot{M}_{\text{CSM}} = 2L \frac{V_{\text{CSM}}}{V_{\text{CDS}}^3} \quad (1.2)$$

One major caveat to this equation is that it requires a constant mass-loss rate and  $V_{\text{CSM}}$  over time in order to have the CSM density decrease as  $r^{-2}$ . If 1.2 is used when the CSM density profile is shallower, it will return a much larger mass-loss rate than is true (Dwarkadas, 2011). A review by Dwarkadas (2011) of several SNe IIn show that their mass-loss rates were overestimated, adding further confusion as to what the progenitors to these explosions are. Additionally, many SNe IIn show signs of significant

asymmetries in their CSM, which will further alter the discrepancies between the results from the equation and the actual star.

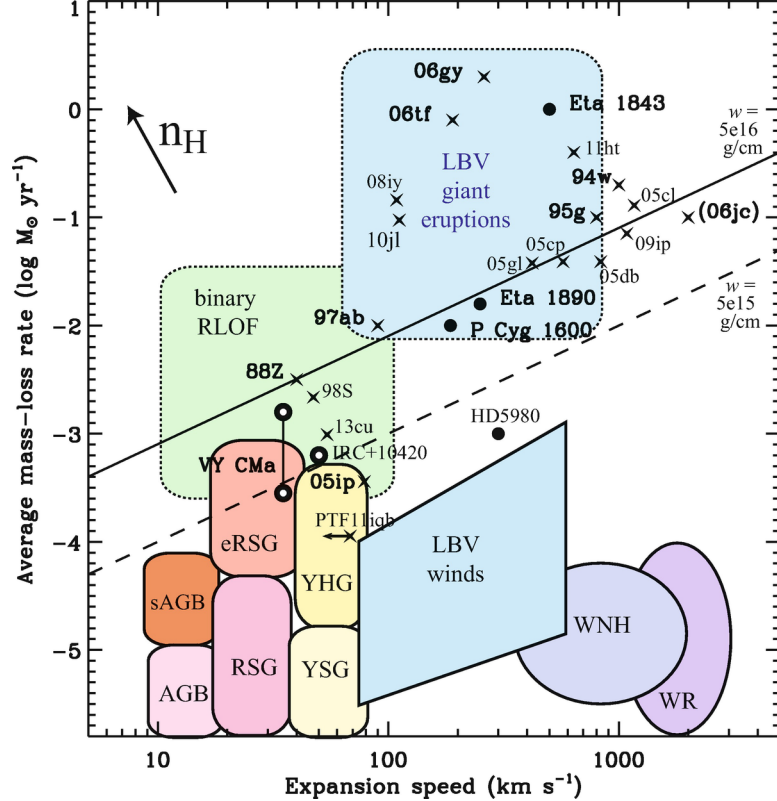


Figure 1.2: Plot of mass-loss rate as a function of wind velocity, with comparisons to known SNe IIn explosions and possible progenitor stars. Observational estimates of different SNe IIn are represented by X's, and some stars with high mass-loss (e.g.  $\eta$  Car) are represented by circles. The patches represent the approximate parameter spaces for different types of stars. Represented in this plot are asymptotic giant branch (AGB) and super-AGB (sAGB) stars, red supergiant (RSG) and extreme-RSGs, yellow super- and hypergiants (YSG, YHG), winds and eruptions from luminous blue variables (LBVs), Wolf Rayet stars (WR, WNH), as well as progenitors arising from basic binary Roche lobe overflow (RLOF). This figure was adapted from Smith (2017).

Even with this setback, conclusions can be made about what kind of stars are able to produce fast enough winds and high enough mass-loss rates seen in SNe IIn. A plot from Smith (2017) comparing mass-loss rate and wind velocities of several SNe IIn and comparing them to progenitor properties can be seen in Fig. 1.2. It is worth noting that

most SNe IIn require some sort of giant luminous blue variable (LBV) eruption in the decades preceding explosion to create enough CSM to form the narrow lines present in SNe IIn.

LBVs are extremely luminous stars which undergo periods of extreme mass loss through violent eruptions (Humphreys and Davidson, 1994), though the cause of such eruptions and their variability are still not well understood. These eruptive events can create a large amount of CSM surrounding the stars, and in the cases of the most luminous LBVs such as  $\eta$  Car and SN 2009ip these explosions can be bright enough to be misinterpreted as SNe (these are known as supernova imposters).

Referring back to Fig. 1.2, we see that while some IIn could arise from binary Roche lobe overflow (RLOF) or extreme red supergiants (eRSGs), it is clear that mass-loss estimates and wind speeds favor an LBV progenitor for most SNe IIn. Indeed, direct observations of progenitors for SNe IIn explosions such as SN 2009ip (Mauerhan et al., 2012, still debated) and SN 2010jl (Smith et al., 2011) appear to show a progenitor LBV in the location of the future explosion, though follow up observations to see if they are just SN imposters in the form of LBV eruptions are not common.

In terms of traditional stellar evolution models, however, having an LBV directly cause a SNe IIn is strongly opposed. These models treat LBVs as a short transition stage for an O-star, with its high mass-loss serving as an important stepping stone for the star to become an H-poor Wolf-Rayet (WR) star (Smith and Owocki, 2006). As mentioned before, Dwarkadas (2011) attempts to circumvent the necessity of a LBV by claiming that a clumpy CSM or an extremely short WR phase can also create the CSM necessary for SNe IIn, but the general consensus remains with LBVs as the main progenitor.

## 1.2 Runaway Stars

One hypothesis presented by Smith and Tombleson (2015) claims that approaching LBVs as runaway stars ejected from a binary system will allow them to become direct progenitors to SNe IIn.

Runaway stars are defined to have space velocities of 30 to 40 km s<sup>-1</sup> (Blaauw, 1961; Eldridge et al., 2011), though some can reach velocities over 200 km s<sup>-1</sup>. As described

in Eldridge et al. (2011), the two main scenarios to create runaway stars are through a dynamical ejection scenario (DES) and through a binary supernova scenario (BSS), though the fastest runaway stars could have been created by a combination of both. In the DES, stars would be ejected via encounters with other massive stars in a dense cluster - this can be single stars or even entire binary systems of stars. The BSS, on the other hand, involves when one of the stars in a binary explodes, unbinding the system and kicking the secondary star. The two methods are expected to contribute roughly equal amounts of runaway stars, but it is possible to differentiate between the two by looking at their compositions as BSS runaways should show evidence of binary interaction (Eldridge et al., 2011). Again, since entire binary systems can be ejected in DES, it is reasonable to assume that some of those binary systems undergo BSS as well.

The most common type of runaway star are O- and B-type stars (Blaauw, 1961), massive stars that can lead to core collapse explosions. Since these stars are launched in excess of  $30 \text{ km s}^{-1}$ , it is not unreasonable that secondary stars kicked in a BSS could travel many parsecs before exploding in their own SN. The simulations run by Eldridge et al. (2011) (seen in Fig. 1.3) do in fact find that for Type II SNe as well as Type Ib and Ic SNe that these progenitors can be launched in excess of 100 pc from the star-forming region they were born in.

While Eldridge et al. (2011) does not look at SNe IIn specifically, Habergham et al. (2014) analyzes 39 SNe IIn and SN imposters and looking to see how they follow H $\alpha$  emission (a tracer of star formation) in their host galaxies. Based on these observations, Habergham et al. (2014) conclude that not only do SNe IIn not correlate to star formation regions, they correlate even less to star formation than other explosions such as SNe II-P. The authors attribute this as an indication that SNe IIn are unlikely to have high mass progenitors, as they expect them to follow star forming regions as well as SN Ic, which have massive progenitors as well. This implies that whatever progenitor is creating Type IIn explosions must either be low enough mass to survive longer than higher mass stars, or they have been isolated by some other means.

Although this appears to be contradictory, observations of LBVs in the Milky Way (MW), Large Magellanic Cloud (LMC), and Small Magellanic Cloud (SMC) imply that LBV stars almost always find themselves isolated from other O-type stars and star-forming regions (Smith and Tombleson, 2015). This matches up nicely with the generally

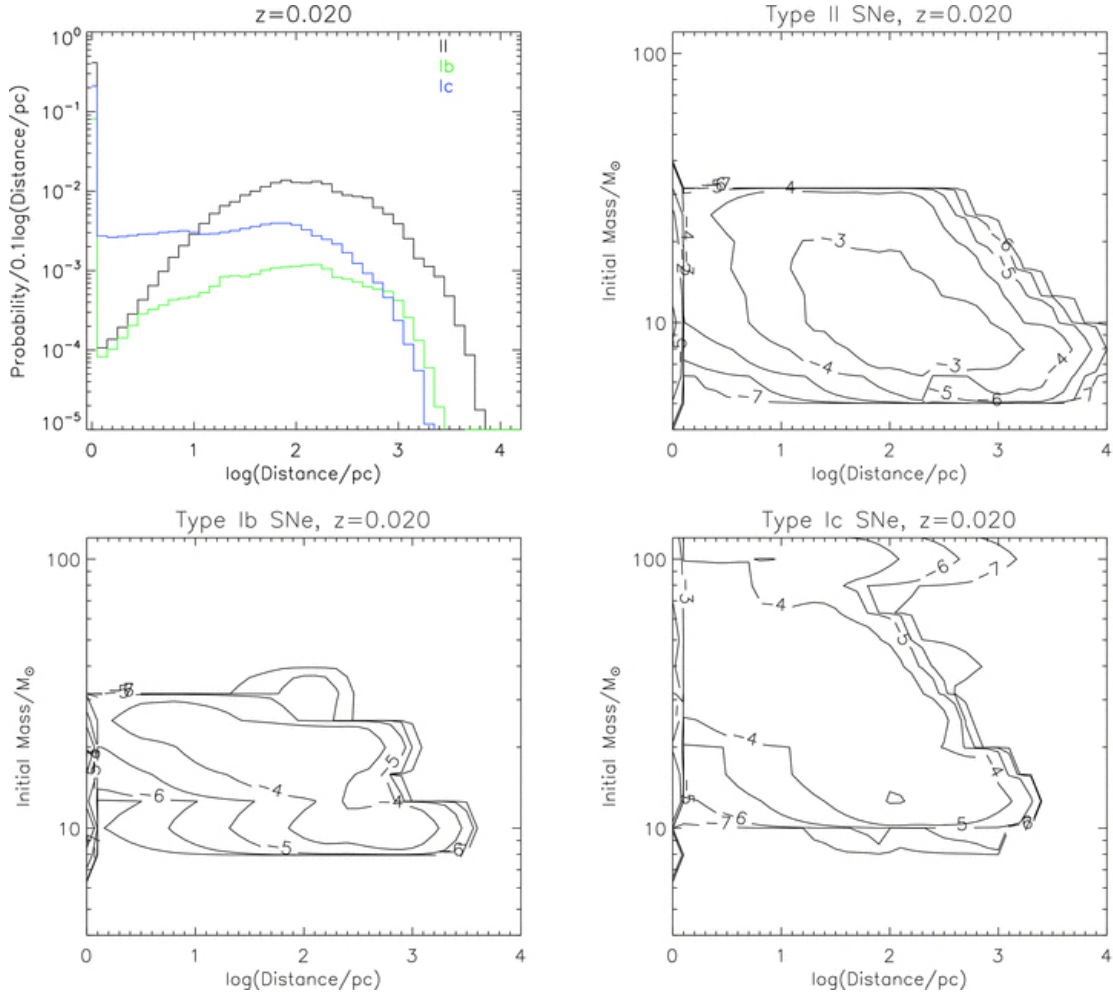


Figure 1.3: Plot showing the distribution of distance traveled by SN progenitors versus the progenitor's original mass, in solar metallicity. The data comes from the simulations of Eldridge et al. (2011). The contours represent the probability in  $\log_{10}$  of a SN progenitor of that initial mass traveling that distance. This figure has been adapted from Eldridge et al. (2011).

accepted view of LBVs serving as the progenitors for SNe IIn.

In order to reconcile the fact that LBVs according to stellar evolution models should not be found isolated, Smith and Tombleson (2015) suggest that most LBV stars are actually the end stage for the kicked mass gaining companion in the BSS. With the LBV progenitor being kicked from its binary, it can then travel the adequate distance to be found later in a region of relative isolation from other O-type stars and star forming regions. The important aspect of this scenario is that the LBV progenitor, serving as the secondary star, accretes mass through RLOF from the primary star prior to the primary star’s explosion. This allows the star to substantially increase its own mass and luminosity, and therefore appear younger than the stars around it (these are known as “blue stragglers”) (Smith and Tombleson, 2015). These stars will still have an extended lifetime compared to stars of their new mass and luminosity, and as such can travel great distances before evolving and exploding (Smith and Tombleson, 2015). Additionally, the process of RLOF will allow them to gain significant angular momentum and velocity, which may be important to LBV instabilities and eruptions (Smith and Tombleson, 2015).

### 1.3 This thesis

The goal of this thesis is to determine if we see evidence of SNe IIn arising from runaway stars, and if so, place constraints on them in the hope of learning more about their progenitors. In order to do this, I will be analyzing the narrow H $\alpha$  lines of SNe IIn and comparing their line of sight velocities to the expected radial velocity of the galaxy in that location.

Chapter 2 will detail the observed supernovae I use in this thesis, as well as how they were obtained. Chapter 3 will talk about the methods used to analyze the offset velocities of the SNe IIn relative to their host galaxies. Chapter 4 will detail the findings of this thesis as well as any future work that can be done from here. Finally, Chapter 5 will conclude the findings of this thesis.

# Chapter 2

## Observations

### 2.1 Observed SNe IIn

All observations used for this thesis were taken with the DEIMOS (DEep Imaging Multi-Object Spectrograph) multi-object spectrograph on the Keck II (10-m) telescope (Faber et al., 2003). In order to collect as many SNe IIn as possible, a list of SNe IIn was obtained using the Asiago Supernova Catalog (Barbon et al., 1999), a catalog of supernovae dating from 1885 to 2017, as well as the Transient Name Server<sup>1</sup> from the International Astronomical Union. These were then searched in the Keck Observatory Archive to see if any observations were taken of the SNe with DEIMOS. Upon analysis, we also removed any SNe IIn that had already evolved to the point where the SN ejecta was freely expanding (there were no more narrow- or intermediate-width H $\alpha$  lines). All observations used in this thesis are listed in Table 2.1. *Of note: many more SN were downloaded than were analyzed due to errors with the DEIMOS pipeline.*

### 2.2 DEIMOS

DEIMOS is a multi-object spectrograph capable of taking spectra of multiple objects at once. The slitmasks span 16.7' of the sky, and have a wavelength range of 4100 Å to 1.1  $\mu$ m (Faber et al., 2003). The observations used in this thesis all utilize the Long Variable Multislit (LVM) slitmask. All observations taken prior to 2008 utilized four

---

<sup>1</sup> <https://wis-tns.weizmann.ac.il/>

SN	Date (UT)	Galaxy Host	Grating Used	PI
SN 2013dz	2013 Aug 2	Unknown	1200G	Filippenko, A.
SN 2013W	2013 Apr 8	UGC 5448	600ZD	Filippenko, A.
SN 2012ab	2012 Nov 15	Unknown	600ZD	Filippenko, A.
SN 2008en	2012 Sep 23	UGC 564	1200G	Filippenko, A.
SN 2010jl	2010 Nov 7	UGC 5189A	600ZD	Filippenko, A.
SN 2005R	2005 Feb 11	UGC 6274	600ZD	Davis, M.

Table 2.1: Table of observations

slitlets on the original LVM, while future ones use the LVMslitB or LVMslitC which have 5 slitlets.

DEIMOS has two separate gratings: a lower-resolution aluminized grating with 600 lines mm<sup>-1</sup> (600ZD) blazed at 7500 Å which offers a width of 5300 Å; and a higher-resolution gold-coated grating with 1200 lines mm<sup>-1</sup> (1200G) blazed at 7500 Å offering a width of 2630 Å.

Fig. 2.1 shows an image of SN 2015bf prior to being reduced in the DEIMOS pipeline. This image is transposed and rotated such that the *x* axis represents wavelength (increasing to the right) and the *y* axis represents the location of the emission. Several night-sky emission lines from the atmosphere can be seen in this image, and are removed in the pipeline.

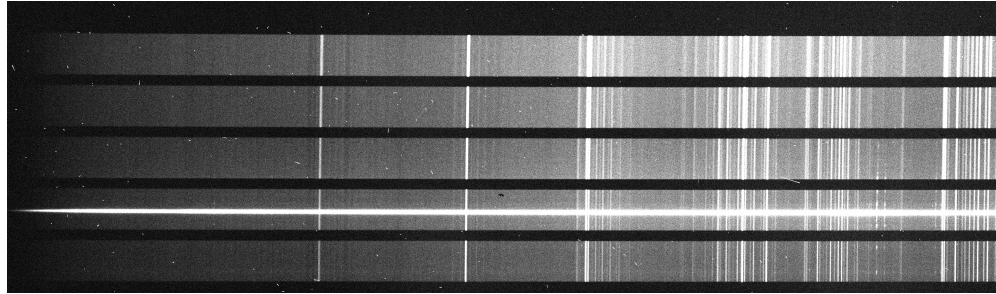


Figure 2.1: An image taken of the blue portion SN 2015bf on DEIMOS, prior to being reduced. This image has transposed and rotated such that the *x* axis represents wavelength (increasing to the right) and the *y* axis represents location in the CCD. The SN continuum is clearly visible in the second slit from the left, though there are many skylines still present. This image was taken as part of the Keck-UC Time-domain Exploration.

## 2.3 H $\alpha$ $\lambda 656\text{nm}$

H $\alpha$  is the primary Balmer line of hydrogen, occurring when a hydrogen electron moves from the third energy level to the second energy level. As mentioned in Chapter 1, we expect to see strong emissions of H $\alpha$  in spectra of SNe IIn due to the shock heating of the CDS. We additionally would expect to see H $\alpha$  tracing the SN host galaxy, as it traces high mass stars and star formation rates (as mentioned in Habergham et al. (2014)). An example H $\alpha$  spectrum from a SNe IIn can be seen in Fig. 2.2 which displays the narrow (and the beginnings of intermediate) width H $\alpha$  emission in SN 2008en.

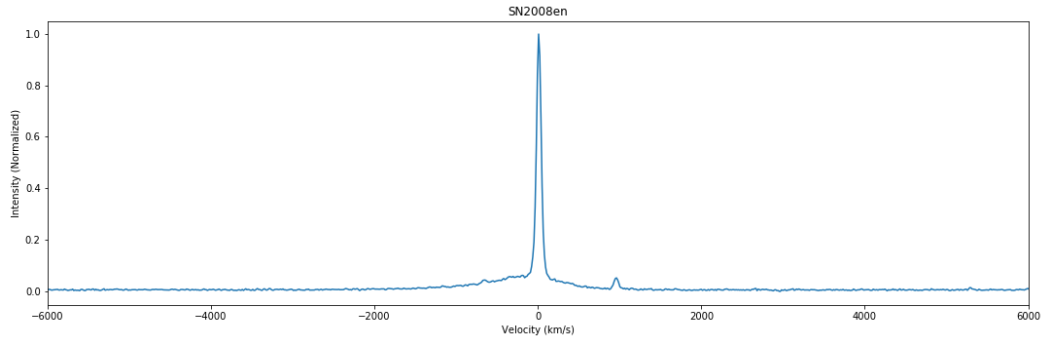


Figure 2.2: Spectrum of the H $\alpha$  emission from SN 2008en. We can see here strong narrow emission lines of H $\alpha$  which is flanked by weak [N II] emission on both sides. There is also a very weak intermediate-width H $\alpha$  emission starting to form (displayed by the slight bump). This image is centered on the narrow H $\alpha$  emission and shows Doppler velocity on the  $x$  axis and normalized flux per unit wavelength on the  $y$  axis.

Since DEIMOS is a multi-object spectrograph we can expect to see the SN continuum, the SN H $\alpha$ , and the host galaxy H $\alpha$  in the same image. An example of this can be seen in Fig. 2.3, which displays the H $\alpha$  of SN 2013dz and its host galaxy. What is typically seen in these observations is a bright continuum emission from the SN, making it difficult to visually distinguish the H $\alpha$  emission. We also see a fainter (though it is not depicted as such in Fig. 2.3) H $\alpha$  emission that traces the host galaxy's emission.

One property of this image that is easy to notice is that the galactic H $\alpha$  shifts from left to right in wavelength. This is expected, as this shift represents the Doppler shift of different parts of the galaxy. In Fig. 2.3, the bottom portion of the galaxy is blueshifted, indicating its line of sight velocity is pointed towards the observer, while the top portion

is redshifted. This shift can be used to estimate what radial velocity is expected of the SN IIn if it were not a runaway star.

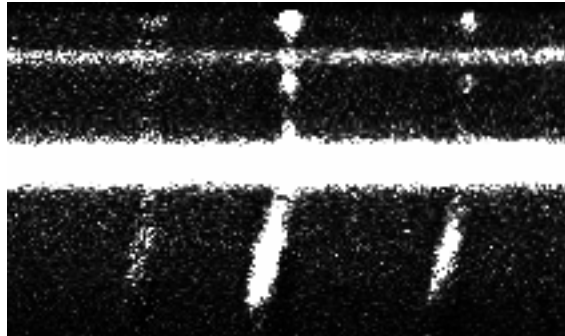


Figure 2.3: An image taken of the red portion of SN 2013dz on DEIMOS, after being reduced. We can clearly see the H $\alpha$  emission from the host galaxy as well as the continuum emission of SN 2013dz. We also can see N II  $\lambda$ 6548 and N II  $\lambda$ 6583 lines of the host galaxy. The H $\alpha$  emission of the SN is difficult to distinguish visually as the SN continuum is already extremely bright.

# Chapter 3

## Analysis

### 3.1 Reducing DEIMOS Images

We used the Carnegie Python Distribution (CarPy)<sup>1</sup> in order to handle, calibrate, reduce, and analyze the images observed from DEIMOS (Kelson et al., 2000; Kelson, 2003). CarPy includes many routines for processing multi-slit spectroscopic data. The CarPy environment also contains PyRAF<sup>2</sup>, a Python based command language to run IRAF<sup>3</sup> (Image Reduction and Analysis Facility) tasks.

Our reduction is based on the standard prescription outlined in Silverman et al. (2012), with slight modifications. Since all of the observations were made on the same instrument (DEIMOS), the only changes that need to be made between different observations is based on the placement of the slitlets, the number of slitlets, and the resolution of the gratings. I will summarize the our pipeline below:

1. Subtract out the overscan region and subtract out the bias. For this, we use `iraf.ccdproc`. Then transpose the image and rotate it 180 degrees such that wavelength is increasing in the  $+x$  direction of the image.
2. Combine and normalize the flat-fields using `iraf.flatcombine`.

---

<sup>1</sup> <https://code.obs.carnegiescience.edu/carnegie-python-distribution>

<sup>2</sup> PyRAF is a product of the Space Telescope Science Institute, which is operated by AURA for NASA.

<sup>3</sup> The Image Reduction and Analysis Facility is distributed by the National Optical Astronomy Observatory, which is operated by the Association of Universities for Research in Astronomy (AURA), Inc., under cooperative agreement with the National Science Foundation (NSF)

3. Rectify the image using the combined flat-fields. The  $y$ -distortion is calculated using `getrect` and then applied to the flats using `copyrect` such that the wavelength in every vertical strip is the same.
4. Find the locations of the slitlets in the images using `findslits`. Once the slits are found, the locations are written to the image header and copied to the rest of the images.
5. Divide out the flat fields and the blaze from the other images using `flat2d`.
6. Get the rectification for each slit using `getrect`, and then copy them to all the other images using `copyrect`. In this step, we are specifically copying the  $x$ -distortion.
7. Calibrate the wavelength scale with `wavrect`. This uses the assistance of arc-lamp spectra, which typically contained Neon, Argon, Krypton, and Xenon, and sometimes Cadmium, Zinc, and Mercury. This gets applied to all the images.
8. Extract the 1D spectra of the standard star using `iraf.apall`. We interactively remove telluric and absorption features using `iraf.splot` to select the regions and then dividing them out using `iraf.sarith`. This forms a standard continuum spectrum, as well as a sensitivity function.
9. Extract the 1D spectra of the SN, and normalize by the standard continuum. Apply telluric corrections using `iraf.telluric`, and flux calibrate using the sensitivity function.
10. Combine the spectra of the blue and red sides to form one complete spectrum. We can then analyze the location of the peak as well as get a full-width half-maximum (FWHM) measurement of the H $\alpha$  using `splot`.

## 3.2 Analyzing Velocities of SNe IIn

Once we are able to extract the spectra, we want to run steps 9 and 10 from Sec. 3.1 for different points of the galaxy’s H $\alpha$  line, as well as on the continuum of the SN to measure the H $\alpha$  emission of the SN. We utilize `splot` to fit a Gaussian or Lorentzian (depending

on which better fits the emission visually) to the emission of H $\alpha$  to determine its central peak and its FWHM. We can then map out the H $\alpha$  emission throughout the galaxy.

With this map, we attempt to fit a cubic polynomial function (reverting to a quadratic for situations where it is not possible, see Fig. B.4 for an example) through the galaxy H $\alpha$  emission. This function provides an estimate for the peak wavelength of the galaxy's H $\alpha$  emission at the location of the supernova, and we can then determine the offset velocity of the SN using a line-of-sight velocity calculation

$$v = \frac{c(\lambda_{\text{gal}} - \lambda_{\text{SN}})}{\lambda_{\text{gal}}} \quad (3.1)$$

where  $v$  is the offset velocity,  $c$  is the speed of light ( $3 \times 10^5$  km s $^{-1}$ ),  $\lambda_{\text{gal}}$  is the estimated wavelength of H $\alpha$  emission of the galaxy at the SN location, and  $\lambda_{\text{SN}}$  is the observed wavelength of the SN H $\alpha$  emission.

Our results for all observed galaxies can be seen in Table 3.1.

SN	Offset (km s $^{-1}$ )	FWHM (km s $^{-1}$ )
SN 2013dz	39.31	82.81
SN 2013W	18.49	261.4
SN 2012ab	13.27	172.5
SN 2010jl	37.46	748.8
SN 2008en	1.98	68.83
SN 2005R	11.16	174.3

Table 3.1: List of SNe IIn, the FWHM of their H $\alpha$  emission, and their offset velocities from their host galaxies.

## Chapter 4

# Discussion

Recalling back to Sec. 1.2, Eldridge et al. (2011) define runaway stars to have space velocities above 30 to 40 km s<sup>-1</sup>. If we look at Table 3.1, we only see two objects that fulfill this definition - SN 2013dz with an offset velocity of 39.31 km s<sup>-1</sup> and SN 2010jl with an offset velocity of 37.46 km s<sup>-1</sup>. All of the other SN have velocities below 20 km s<sup>-1</sup>.

*Basically everything after this could change if I can get the pipeline working for the rest... but I'm going to write it as if nothing will work.*

This data, and more significantly the amount of it we have, makes it extremely difficult to come to any significant conclusions. Having only six data points to work with means that it is unreasonable and irresponsible to claim that many SNe IIn arise from runaway LBVs - but the presence of SN 2013dz and SN 2010jl does give it credence.

### 4.1 Runaway Candidates

#### 4.1.1 SN 2010jl

Smith et al. (2011) goes into detail about the progenitor star of SN 2010jl, as it is one of a few SNe IIn with direct observations of the progenitor prior to explosion. Hubble Space Telescope (HST) observations of the progenitor show a luminous and blue point source at the location of the SN, implying that the progenitor could have been in a massive young star cluster or a quiescent LBV. Combining this with the offset velocity

of SN 2010jl, it is reasonable to suggest that the progenitor was an LBV.

However, it is harder to reconcile the predicted initial mass of  $80 M_{\odot}$  with a runaway, which is expected to be the less massive mass-gaining companion. This mass falls on the higher end of expected runaway masses in Smith and Tombleson (2015), if a star with initial mass of  $30 - 40 M_{\odot}$  accretes enough mass to appear as  $60 - 80 M_{\odot}$  LBVs. It is certainly not unreasonable to claim that the predicted progenitor mass, the observed offset velocity, and observations of the spectrum imply a runaway LBV progenitor, but it is pushing at the lower limits of runaway stars and the higher limits of mass-gaining RLOF stars.

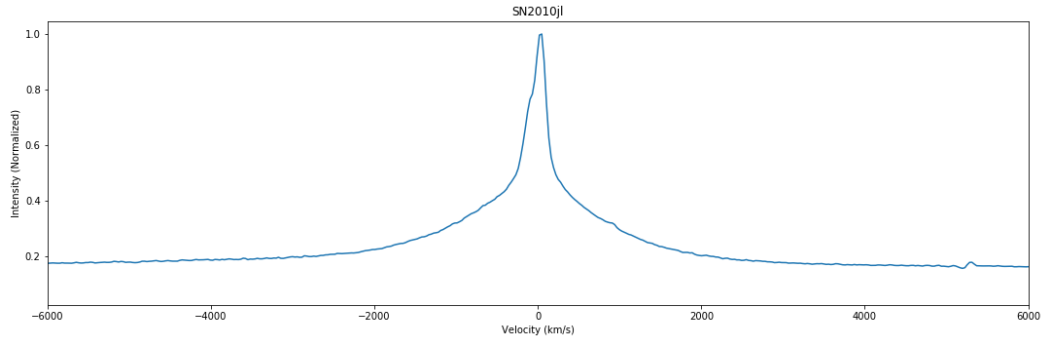


 figure 4.1: Spectrum of the H $\alpha$  emission from SN 2010jl. This spectra appears to show a narrow absorption line overlaid on an intermediate-width line.

#### 4.1.2 SN 2013dz

Unlike SN 2010jl, there are no references to SN 2013dz in scientific literature. It was discovered by Dhungana et al. (2013) in July 2013 and observed again 20 days later using DEIMOS. The one dimensional spectrum can be seen in Fig. 4.2. In it, there is blueshifted hydrogen component and P-Cygni absorption that bears strong similarities to the blueshifted components of SN 2013L, especially in early times (Andrews et al., 2017, see their Fig. 8, 9). Andrews et al. (2017) claim that this suggests that the SN ejecta began interacting with very dense CSM at this time (approximately 30 d after explosion). If we take the date of first observation by Dhungana et al. (2013) as approximately 10 d after explosion, this timeline matches up exactly with SN 2013L.

Andrews et al. (2017) further analyze the evolution of the spectrum of SN 2013L and come to the conclusion that the progenitor star must have had extremely asymmetric CSM in order to generate the H $\alpha$  profile, suggesting an initial mass of  $M > 25M_{\odot}$ . They also suggest that the asymmetry could be a result of binary RLOF, which aligns well with the hypothesis of the progenitor being a BSS runaway. Andrews et al. (2017) also derive a mass-loss rate for the progenitor of SN 2013L being between  $1 \times 10^{-4}$  and  $1 \times 10^{-3}M_{\odot} \text{ yr}^{-1}$ , implying a yellow hypergiant or quiescent LBV.

While we clearly cannot take their results and apply it to SN 2013dz, the similarities in the H $\alpha$  profile do lend their hand to SN 2013dz's progenitor being a runaway star. The peak of the H $\alpha$  emission is at 6881.35 Å, giving a redshift of 0.04629. Using the cosmological parameters from the Planck 2015 survey (Ade et al., 2016) gives an luminosity distance of  $D_L = 212 \text{ Mpc}$ . Taking the FWHM of the P-Cygni absorption as  $V_{\text{CSM}} = 24 \text{ km s}^{-1}$ , taking a rough estimate of the FWHM of the broader H $\alpha$  emission as  $V_{\text{SN}} \approx 536 \text{ km s}^{-1}$  and a luminosity  $L = 0.5L_{\text{H}\alpha} = 0.5 \times 4\pi(212 \text{ Mpc})^2 = 2.635 \times 10^{40} \text{ erg s}^{-1}$ , we can estimate a mass-loss rate of  $\dot{M} \approx 6.513 \times 10^{-3}M_{\odot} \text{ yr}^{-1}$ . It is again important to remember that with an asymmetric CSM we do not have a density profile of  $r^{-2}$ , and as such our estimates may be misrepresenting (Dwarkadas, 2011).

Referring back to Fig. 1.2, we see that this places our progenitor quite safely in the binary RLOF region. Between this and the similarities to SN 2013L, it can reasonably be implied that while not the result of an eruptive LBV, the progenitor could have been ejected through BSS after gaining significant mass and CSM through RLOF.

## 4.2 Implications on progenitors

Even with such a small sample, having two candidates for runaway progenitors is scientifically interesting. It is also fair to claim that projection effects may be at play with some other SNe IIn, as their ejection may not be directly towards or away from the observer. A lack of observed Doppler velocity difference may be a result of the progenitor not being ejected through BSS or DES, or it could be the result of the progenitor simply being ejected in a direction that we cannot discern a velocity through Doppler shift. Due to the large distances to some of these objects it would be difficult to do a survey similar to Habergham et al. (2014) of these events, observing the relative isolation and

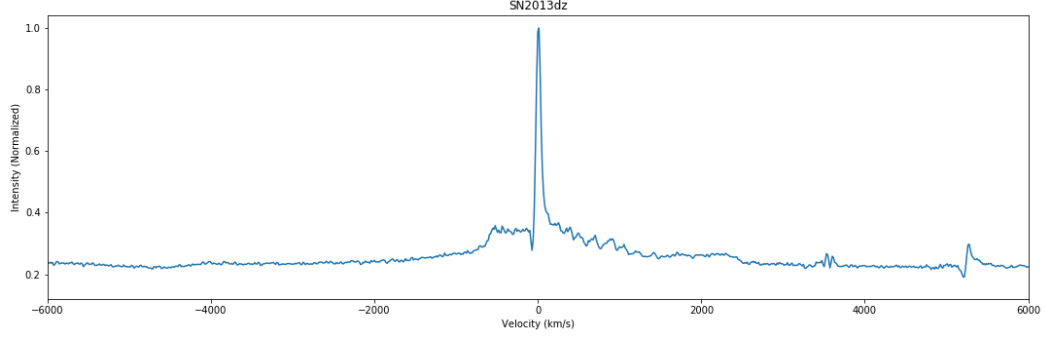


Figure 4.2: 1-D spectrum of SN 2013dz taken by DEIMOS. The absorption on the blueshifted portion of the H $\alpha$  emission has similarities to SN 2013L early in its evolution (Andrews et al., 2017). There does appear to be a strong narrow H $\alpha$  emission line overlaid on an intermediate-width emission, but the absorption on the blue side makes the spectrum resemble a plateau.

distribution of such events.

With that being said, it is important to recall that SNe IIn are external phenomena and do not necessarily arise from a single type of progenitor. Any astrophysical event that leads to significant CSM surrounding a progenitor can lead to a SN IIn event, and as such we should not expect every SN IIn to arise from a runaway LBV.

# **Chapter 5**

## **Conclusion**

Meh. Maybe??? Hard to say. Some of the sample does show it. Some don't. This is expected. We have some that could be good candidates for this scenario, but even there there is still uncertainty. Describe briefly some of the evidence for 2010jl and 2013dz. Not sure how comfortable I am writing this up since we might be able to get more data?

Future could use more observations of IIn, more theoretical work into the evolution of these runaway stars into LBVs.

# References

P. A.R. Ade, N. Aghanim, M. Arnaud, M. Ashdown, J. Aumont, C. Baccigalupi, A. J. Banday, R. B. Barreiro, J. G. Bartlett, N. Bartolo, E. Battaner, R. Battye, K. Benabed, A. Benoît, A. Benoit-Lévy, J. P. Bernard, M. Bersanelli, P. Bielewicz, J. J. Bock, A. Bonaldi, L. Bonavera, J. R. Bond, J. Borrill, F. R. Bouchet, F. Boulanger, M. Bucher, C. Burigana, R. C. Butler, E. Calabrese, J. F. Cardoso, A. Catalano, A. Challinor, A. Chamballu, R. R. Chary, H. C. Chiang, J. Chluba, P. R. Christensen, S. Church, D. L. Clements, S. Colombi, L. P.L. Colombo, C. Combet, A. Coulais, B. P. Crill, A. Curto, F. Cuttaia, L. Danese, R. D. Davies, R. J. Davis, P. De Bernardis, A. De Rosa, G. De Zotti, J. Delabrouille, F. X. Désert, E. Di Valentino, C. Dickinson, J. M. Diego, K. Dolag, H. Dole, S. Donzelli, O. Doré, M. Douspis, A. Ducout, J. Dunkley, X. Dupac, G. Efstathiou, F. Elsner, T. A. Enßlin, H. K. Eriksen, M. Farhang, J. Fergusson, F. Finelli, O. Forni, M. Frailis, A. A. Fraisse, E. Franceschi, A. Frejsel, S. Galeotta, S. Galli, K. Ganga, C. Gauthier, M. Gerbino, T. Ghosh, M. Giard, Y. Giraud-Héraud, E. Giusarma, E. Gjerløw, J. González-Nuevo, K. M. Górski, S. Gratton, A. Gregorio, A. Gruppuso, J. E. Gudmundsson, J. Hamann, F. K. Hansen, D. Hanson, D. L. Harrison, G. Helou, S. Henrot-Versillé, C. Hernández-Monteagudo, D. Herranz, S. R. Hildebrandt, E. Hivon, M. Hobson, W. A. Holmes, A. Hornstrup, W. Hovest, Z. Huang, K. M. Huffenberger, G. Hurier, A. H. Jaffe, T. R. Jaffe, W. C. Jones, M. Juvela, E. Keihänen, R. Keskitalo, T. S. Kisner, R. Kneissl, J. Knoche, L. Knox, M. Kunz, H. Kurki-Suonio, G. Lagache, A. Lähteenmäki, J. M. Lamarre, A. Lasenby, M. Lattanzi, C. R. Lawrence, J. P. Leahy, R. Leonardi, J. Lesgourges, F. Levrier, A. Lewis, M. Liguori, P. B. Lilje, M. Linden-Vørnle, M. López-Caniego, P. M. Lubin, J. F. Maciás-Pérez, G. Maggio, D. Maino, N. Mandolesi,

A. Mangilli, A. Marchini, M. Maris, P. G. Martin, M. Martinelli, E. Martínez-González, S. Masi, S. Matarrese, P. Mcgehee, P. R. Meinhold, A. Melchiorri, J. B. Melin, L. Mendes, A. Mennella, M. Migliaccio, M. Millea, S. Mitra, M. A. Miville-Deschénes, A. Moneti, L. Montier, G. Morgante, D. Mortlock, A. Moss, D. Munshi, J. A. Murphy, P. Naselsky, F. Nati, P. Natoli, C. B. Netterfield, H. U. Nørgaard-Nielsen, F. Noviello, D. Novikov, I. Novikov, C. A. Oxborrow, F. Paci, L. Pagano, F. Pajot, R. Paladini, D. Paoletti, B. Partridge, F. Pasian, G. Patanchon, T. J. Pearson, O. Perdereau, L. Perotto, F. Perrotta, V. Pettorino, F. Piacentini, M. Piat, E. Pierpaoli, D. Pietrobon, S. Plaszczynski, E. Pointecouteau, G. Polenta, L. Popa, G. W. Pratt, G. Prézeau, S. Prunet, J. L. Puget, J. P. Rachen, W. T. Reach, R. Rebolo, M. Reinecke, M. Remazeilles, C. Renault, A. Renzi, I. Ristorcelli, G. Rocha, C. Rosset, M. Rossetti, G. Roudier, B. Rouillé D'orfeuil, M. Rowan-Robinson, J. A. Rubinó-Martín, B. Rusholme, N. Said, V. Salvatelli, L. Salvati, M. Sandri, D. Santos, M. Savelainen, G. Savini, D. Scott, M. D. Seiffert, P. Serra, E. P.S. Shellard, L. D. Spencer, M. Spinelli, V. Stolyarov, R. Stompor, R. Sudiwala, R. Sunyaev, D. Sutton, A. S. Suur-Uski, J. F. Sygnet, J. A. Tauber, L. Terenzi, L. Toffolatti, M. Tomasi, M. Tristram, T. Trombetti, M. Tucci, J. Tuovinen, M. Türler, G. Umana, L. Valentziano, J. Valiviita, F. Van Tent, P. Vielva, F. Villa, L. A. Wade, B. D. Wandelt, I. K. Wehus, M. White, S. D.M. White, A. Wilkinson, D. Yvon, A. Zacchei, and A. Zonca. Planck 2015 results: XIII. Cosmological parameters. *Astronomy and Astrophysics*, 594, 10 2016. ISSN 14320746. doi: 10.1051/0004-6361/201525830.

Jennifer E. Andrews, Nathan Smith, Curtis McCully, Ori D. Fox, S. Valenti, and D. A. Howell. Optical and IR observations of SN 2013L, a Type IIn Supernova surrounded by asymmetric CSM. *Monthly Notices of the Royal Astronomical Society*, 471(4): 4047–4059, 7 2017. ISSN 13652966. doi: 10.1093/MNRAS/STX1844.

R. Barbon, V. Buondí, E. Cappellaro, and M. Turatto. The Asiago Supernova Catalogue - 10 years after. *Astronomy and Astrophysics Supplement Series*, 139(3):531–536, 11 1999. ISSN 03650138. doi: 10.1051/aas:1999404.

A. Blaauw. On the origin of the O and B-type stars with high velocities. *Bulletin of the Astronomical Institutes of the Netherlands*, 15:265, 1961. ISSN 0004-6361.

- G. Dhungana, J. M. Silverman, W. Zheng, R. Kehoe, F. V. Ferrante, J. Vinko, G. H. Marion, R. Quimby, F. Yuan, J. C. Wheeler, and C. Akerlof. Supernova 2013dz. *CBET*, 3589:1, 2013.
- V. Dwarkadas. On luminous blue variables as the progenitors of core-collapse supernovae, especially Type IIn supernovae. *Monthly Notices of the Royal Astronomical Society*, 412(3):1639–1649, 4 2011. ISSN 00358711. doi: 10.1111/j.1365-2966.2010.18001.x.
- John J. Eldridge, Norbert Langer, and Christopher A. Tout. Runaway stars as progenitors of supernovae and gamma-ray bursts. *Monthly Notices of the Royal Astronomical Society*, 414(4):3501–3520, 3 2011. ISSN 00358711. doi: 10.1111/j.1365-2966.2011.18650.x.
- Sandra M. Faber, Andrew C. Phillips, Robert I. Kibrick, Barry Alcott, Steven L. Allen, Jim Burrous, T. Cantrall, De Clarke, Alison L. Coil, David J. Cowley, Marc Davis, William T. S. Deich, Ken Dietsch, David K. Gilmore, Carol A. Harper, David F. Hilyard, Jeffrey P. Lewis, Molly McVeigh, Jeffrey Newman, Jack Osborne, Ricardo Schiavon, Richard J. Stover, Dean Tucker, Vernon Wallace, Mingzhi Wei, Gregory Wirth, and Christopher A. Wright. The DEIMOS spectrograph for the Keck II Telescope: integration and testing. In Masanori Iye and Alan F. M. Moorwood, editors, *Instrument Design and Performance for Optical/Infrared Ground-based Telescopes*, volume 4841, page 1657. SPIE, 3 2003. doi: 10.1117/12.460346.
- S. M. Habergham, J. P. Anderson, P. A. James, and J. D. Lyman. Environments of interacting transients: Impostors and Type IIn supernovae. *Monthly Notices of the Royal Astronomical Society*, 441(3):2230–2252, 4 2014. ISSN 13652966. doi: 10.1093/mnras/stu684.
- Roberta M. Humphreys and Kris Davidson. The luminous blue variables: Astrophysical geysers. *Publications of the Astronomical Society of the Pacific*, 106:1025, 10 1994. ISSN 0004-6280. doi: 10.1086/133478.
- Daniel D. Kelson, Garth D. Illingworth, Pieter G. van Dokkum, and Marijn Franx. The Evolution of Early-Type Galaxies in Distant Clusters. II. Internal Kinematics

of 55 Galaxies in the Cluster Cl 1358+62. *The Astrophysical Journal*, 531(1):159–183, 8 2000. ISSN 0004-637X. doi: 10.1086/308445. URL <http://arxiv.org/abs/astro-ph/9908257><http://dx.doi.org/10.1086/308445>.

Daniel D. Kelson. Optimal Techniques in Two-dimensional Spectroscopy: Background Subtraction for the 21st Century. *Publications of the Astronomical Society of the Pacific*, 115(808):688–699, 6 2003. ISSN 0004-6280. doi: 10.1086/375502.

Jon C. Mauerhan, Nathan Smith, Alexei Filippenko, Kyle Blanchard, Peter Blanchard, Chadwick F. E. Casper, S. Bradley Cenko, Kelsey I. Clubb, Daniel Cohen, Kiera Fuller, Gary Li, and Jeffrey M. Silverman. The Unprecedented 2012 Outburst of SN 2009ip: A Luminous Blue Variable Becomes a True Supernova. 9 2012. doi: 10.1093/mnras/stt009. URL <http://arxiv.org/abs/1209.6320><http://dx.doi.org/10.1093/mnras/stt009><http://arxiv.org/abs/1209.6320%0A><http://dx.doi.org/10.1093/mnras/stt009>.

E. Schlegel. A new subclass of type II supernovae? *Monthly Notices of the Royal Astronomical Society*, 244(2):269–271, 1990. ISSN 0035-8711.

Jeffrey M. Silverman, Ryan J. Foley, Alexei V. Filippenko, Mohan Ganeshalingam, Aaron J. Barth, Ryan Chornock, Christopher V. Griffith, Jason J. Kong, Nicholas Lee, Douglas C. Leonard, Thomas Matheson, Emily G. Miller, Thea N. Steele, Brian J. Barris, Joshua S. Bloom, Bethany E. Cobb, Alison L. Coil, Louis Benoit Desroches, Elinor L. Gates, Luis C. Ho, Saurabh W. Jha, Michael T. Kandrashoff, Weidong Li, Kaisey S. Mandel, Maryam Modjaz, Matthew R. Moore, Robin E. Mostardi, Marina S. Papenkova, Sung Park, Daniel A. Perley, Dovi Poznanski, Cassie A. Reuter, James Scala, Franklin J.D. Serduke, Joseph C. Shields, Brandon J. Swift, John L. Tonry, Schuyler D. Van Dyk, Xiaofeng Wang, and S. Diane. Berkeley Supernova Ia Program - I. Observations, data reduction and spectroscopic sample of 582 low-redshift Type Ia supernovae. *Monthly Notices of the Royal Astronomical Society*, 425(3):1789–1818, 9 2012. ISSN 00358711. doi: 10.1111/j.1365-2966.2012.21270.x.

Nathan Smith. Interacting Supernovae: Types IIn and Ibn. In *Handbook of Supernovae*, pages 403–429. Springer International Publishing, 12 2017. doi: 10.1007/978-3-319-21846-5\\_{\}-}38.

Nathan Smith and Stanley P. Owocki. On the Role of Continuum-driven Eruptions in the Evolution of Very Massive Stars and Population III Stars. *The Astrophysical Journal*, 645(1):L45–L48, 7 2006. ISSN 0004-637X. doi: 10.1086/506523.

Nathan Smith and Ryan Tombleson. Luminous blue variables are antisocial: Their isolation implies that they are kicked mass gainers in binary evolution. *Monthly Notices of the Royal Astronomical Society*, 447(1):598–617, 6 2015. ISSN 13652966. doi: 10.1093/mnras/stu2430.

Nathan Smith, Ryan Chornock, Weidong Li, Mohan Ganeshalingam, Jeffrey M. Silverman, Ryan J. Foley, Alexei V. Filippenko, and Aaron J. Barth. SN 2006tf: Precursor Eruptions and the Optically Thick Regime of Extremely Luminous Type IIn Supernovae. *The Astrophysical Journal*, 686(1):467–484, 10 2008. ISSN 0004-637X. doi: 10.1086/591021.

Nathan Smith, Weidong Li, Adam A. Miller, Jeffrey M. Silverman, Alexei V. Filippenko, Jean Charles Cuillandre, Michael C. Cooper, Thomas Matheson, and Schuyler D. Van Dyk. A massive progenitor of the luminous type IIn supernova 2010jl. *Astrophysical Journal*, 732(2), 11 2011. ISSN 15384357. doi: 10.1088/0004-637X/732/2/63.

## Appendix A

# Glossary and Acronyms

Care has been taken in this thesis to minimize the use of jargon, but this cannot always be achieved. This appendix defines jargon terms in a glossary, and contains a table of acronyms and their meaning.

### A.1 Glossary

CSM, SN, LBV, RLOF, BSS, DES , FWHM,  $M_{\odot}$ , roche lobe, light curve, blazed grating  
DEIMOS, HST, LVM, IRAF

- **Object** – definition

## A.2 Acronyms

Table A.1: Acronyms

Acronym	Meaning
BSS	Binary Supernova Scenario
CSM	CircumStellar Material
DEIMOS	DEep Imaging Multi-Object Spectrograph
DES	Dynamical Ejection Scenario
HST	Hubble Space Telescope
IRAF	Image Reduction and Analysis Facility
LBV	Luminous Blue Variable
LVM	Long View Mirror
RLOF	Roche Lobe OverFlow
SN	SuperNova (plural SNe, SuperNovae)
SNe IIn	SuperNova type IIn

## Appendix B

# Images and Spectra

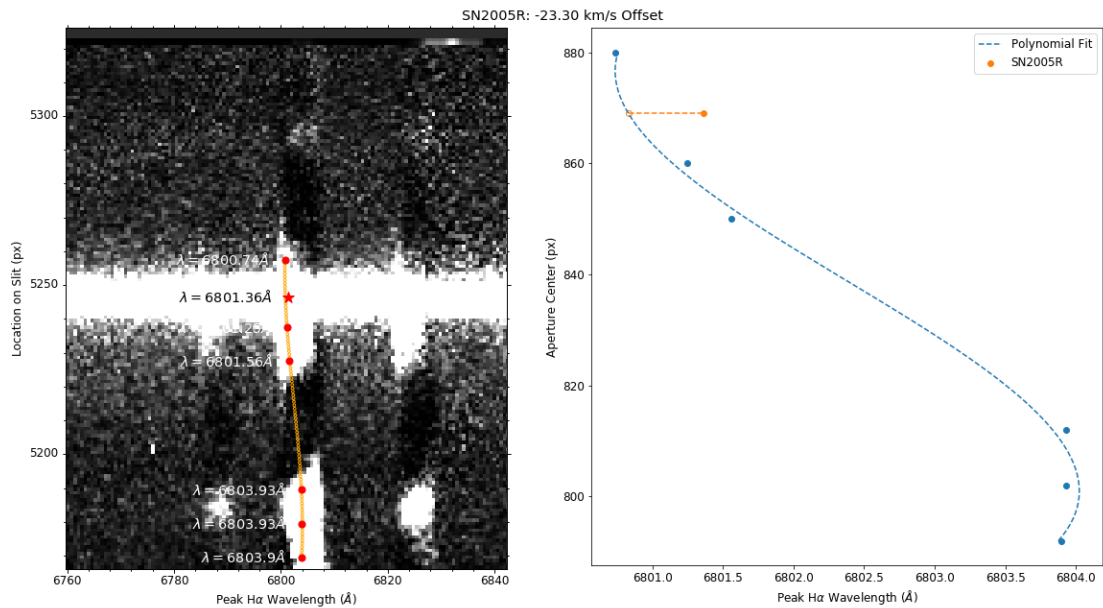
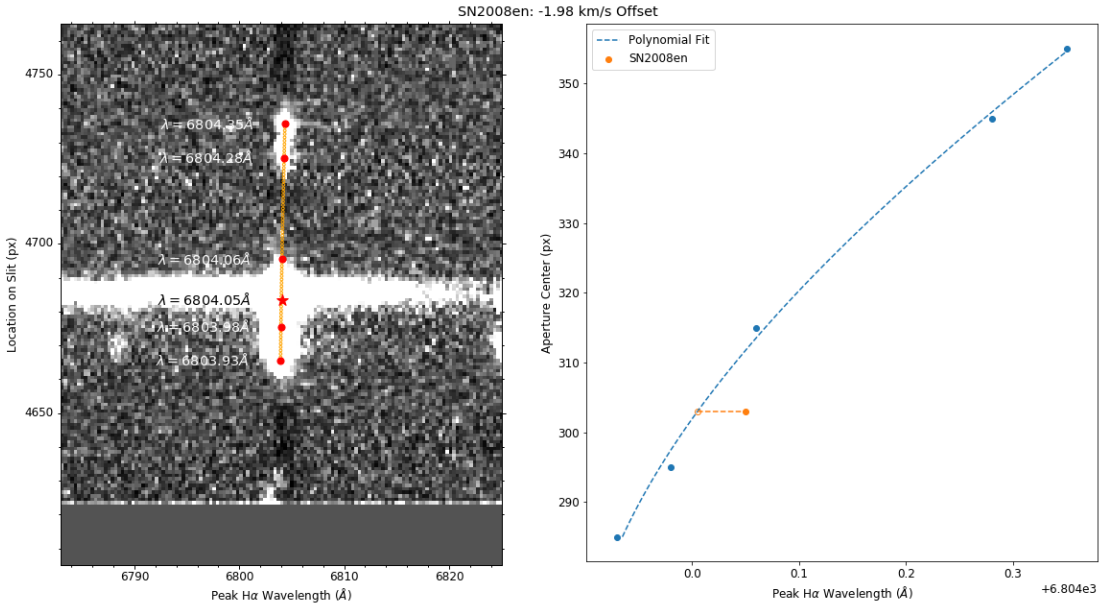
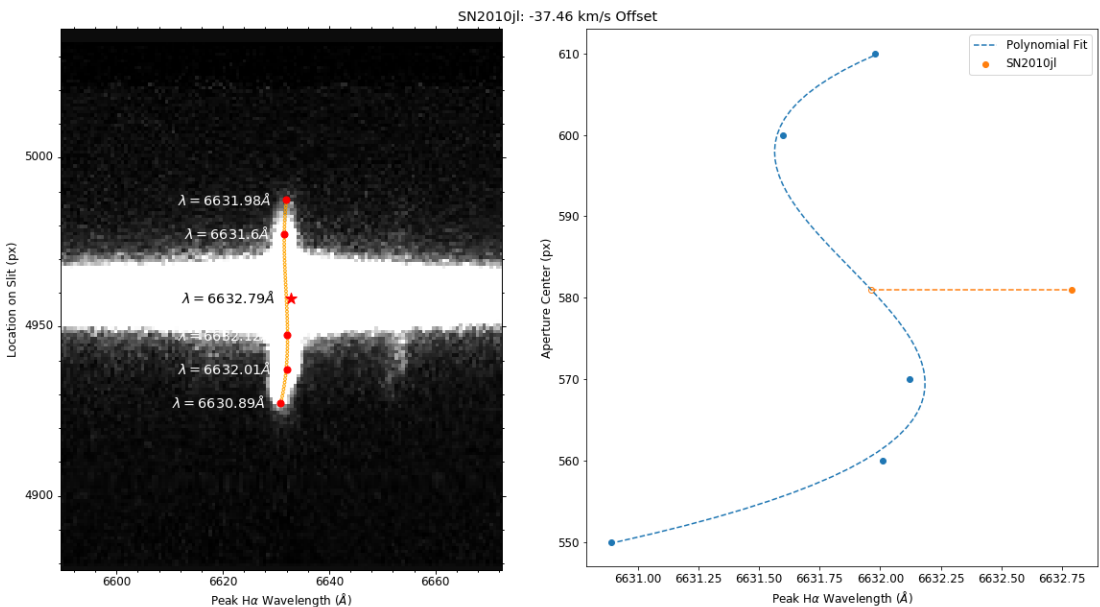
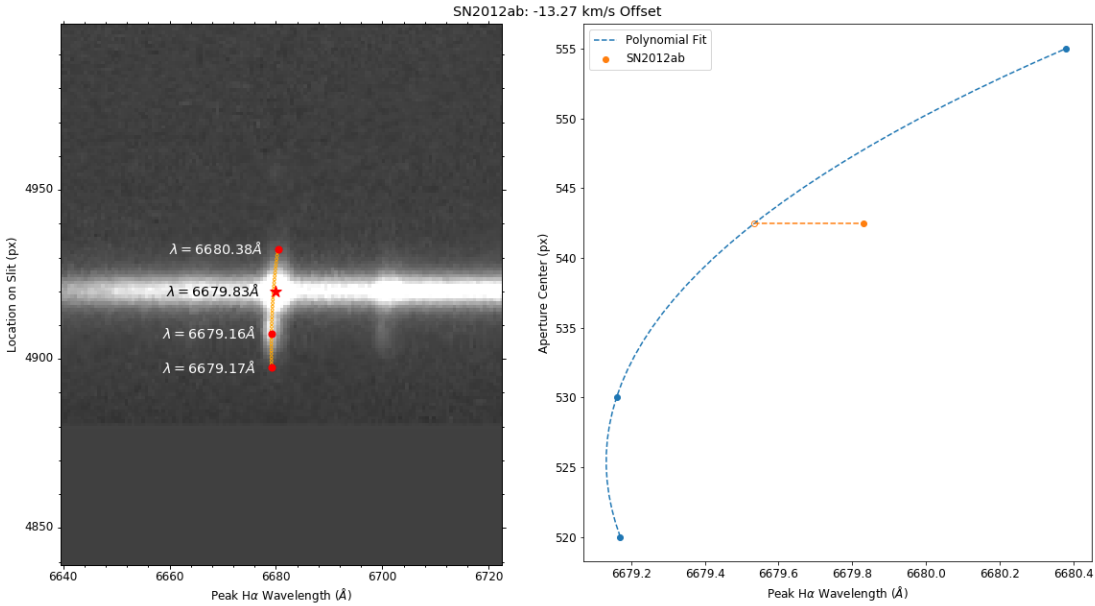
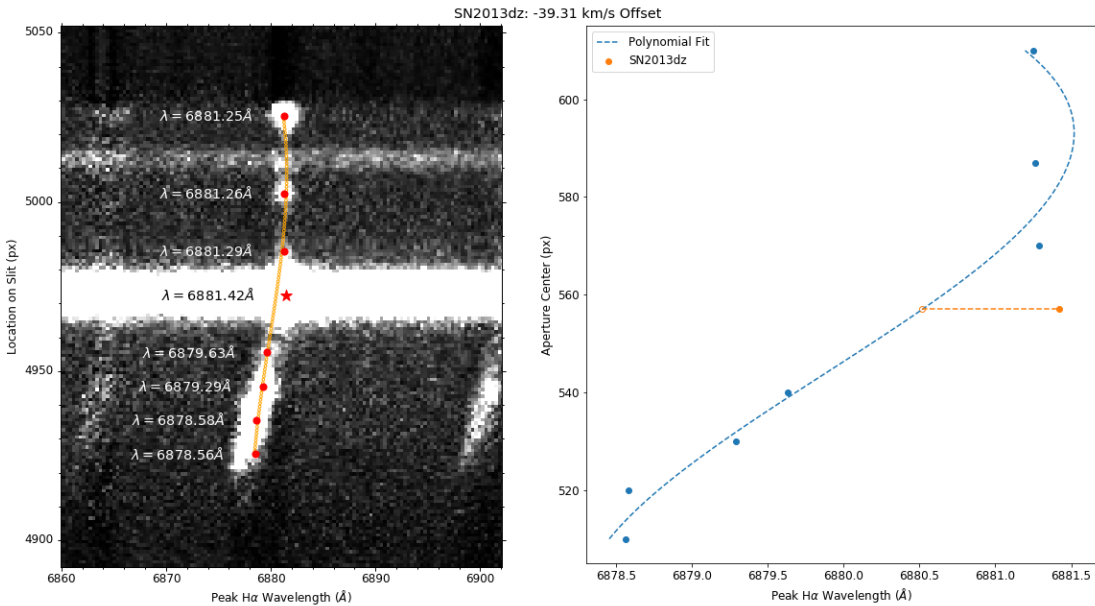


Figure B.1: SN 2005R H $\alpha$  relative to host galaxy

Figure B.2: SN 2008en H $\alpha$  relative to host galaxyFigure B.3: SN 2010jl H $\alpha$  relative to host galaxy

Figure B.4: SN 2012ab H $\alpha$  relative to host galaxyFigure B.5: SN 2013dz H $\alpha$  relative to host galaxy

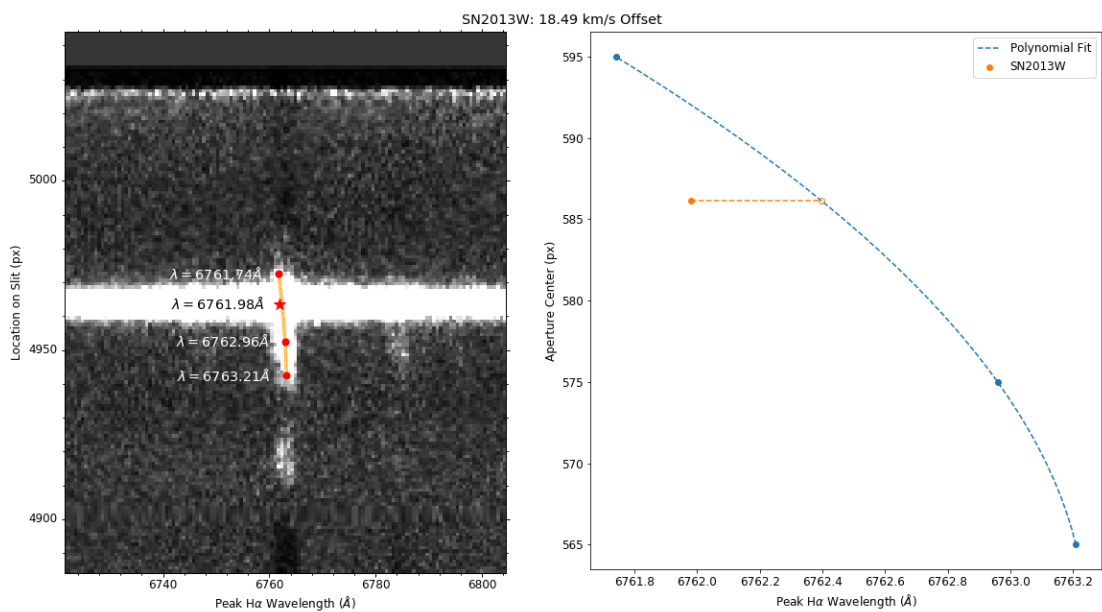


Figure B.6: SN 2013W H $\alpha$  relative to host galaxy